effective for the criterion of eqn. 3. $|\boldsymbol{k}_1 - \boldsymbol{k}_0|$ is nearly equal to $|\boldsymbol{k}_2 - \boldsymbol{k}_0|$, the energies of the wave vectors of electrons diminished by $\boldsymbol{k}_0$ are therefore an effective criterion. They can be calculated by the relation $(h^2/2m_\Gamma^*)k^2 = \varepsilon(1 + \alpha_\Gamma \varepsilon)$ for the Γ-valley, where m_Γ^* and α_Γ are the effective mass and nonparabolicity, respectively. Define an energy denoted by $\varepsilon_\Gamma'(\boldsymbol{r}, t)$. This is a mean energy averaged over the energies of the wave vectors subtracted by $\boldsymbol{k}_0$ for all the Γ-valley electrons. It can be given by the following expression:

$$\varepsilon_\Gamma'(\boldsymbol{r}, t) = \int_0^\infty \varepsilon g_\Gamma(\varepsilon) f(\varepsilon, \boldsymbol{r}, t)\, d\varepsilon / n_\Gamma(\boldsymbol{r}, t) \tag{5}$$

Using the approximation

$$(1 + \alpha_\Gamma k_B T_e y)^{1/2} = 1 + \tfrac{1}{2}\alpha_\Gamma k_B T_e y$$

eqns. 2 and 5 are rewritten as

$$n_\Gamma(\boldsymbol{r}, t) = A[\Gamma(\tfrac{3}{2})F_{1/2}(y_0) + \tfrac{5}{2}\alpha_\Gamma k_B T_e(\boldsymbol{r}, t)\Gamma(\tfrac{5}{2})F_{3/2}(y_0)] \tag{6a}$$

$$\varepsilon_\Gamma'(\boldsymbol{r}, t) = k_B T_e(\boldsymbol{r}, t) \times \frac{\Gamma(\frac{5}{2})F_{3/2}(y_0) + \frac{5}{2}\alpha_\Gamma k_B T_e(\boldsymbol{r}, t)\Gamma(\frac{7}{2})F_{5/2}(y_0)}{\Gamma(\frac{3}{2})F_{1/2}(y_0) + \frac{5}{2}\alpha_\Gamma k_B T_e(\boldsymbol{r}, t)\Gamma(\frac{5}{2})F_{3/2}(y_0)} \tag{6b}$$

where

$$A = [2m_\Gamma^* k_B T_e(\boldsymbol{r}, t)]^{3/2}/(2\pi^2 h^3)$$

$$y = \varepsilon / k_B T_e(\boldsymbol{r}, t)$$

$$y_0 = \varepsilon_f(\boldsymbol{r}, t)/k_B T_e(\boldsymbol{r}, t)$$

Γ is the Gamma function, and F_j is the Fermi–Dirac integral of order j defined by

$$F_j(y_0) = \int_0^\infty \frac{y^j\, dy}{1 + \exp(y - y_0)} \Big/ \Gamma(j + 1)$$

From eqns. 6*a* and *b*, an equation for y_0 may be obtained namely $\varepsilon_f(\boldsymbol{r}, t)$, which can be numerically solved. $T_e(\boldsymbol{r}, t)$ is calculated by eqn. 6*b*.

To show effectiveness of eqns. 6*a* and *b*, simulation results under a uniform electric field are presented. The carrier–carrier interaction is not taken into consideration for simplicity. In the Figures the results are obtained for the carrier concentration of $2 \times 10^{18}\,\mathrm{cm}^{-3}$ and the electric fields of 2kV/cm and 7kV/cm at 300K. Fig. 2 shows the time responses of the mean velocity. Good agreements between the present method using eqn. 5 and the exact algorithm of Lugli and Ferry are observed. The previous method using eqn. 4 produces a larger mean velocity than the exact algorithm. There is not a large difference among the three methods for the mean energy. The electron distribution function, specified as a function of k_z which is the component of $\boldsymbol{k}$ along the electric field, has also been studied. It has been confirmed that the distribution function obtained by the present method agrees well with that obtained by the exact algorithm. The distribution function obtained by the previous method was shifted by a small amount to the positive direction of k_z. This corresponds to the larger mean velocity shown in Fig. 2. The present method is a better approximation than the previous one for a wide range of the carrier concentration. It may therefore be effective for device simulation.

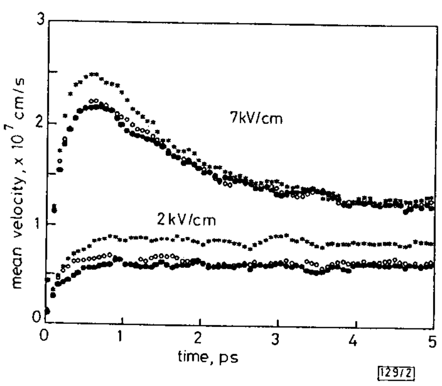

Fig. 2 *Time responses of mean velocity under uniform electric fields*
300K; $2 \times 10^{18}\,\mathrm{cm}^{-3}$
○ Lugli and Ferry
● proposed method
∗ Fischetti and Laux

Acknowledgments: The author would like to express thanks to Y. Matsuguma and Y. Koura for their technical assistance.

Y. YAMADA

12th February 1991

Department of Electrical Engineering and Computer Science
Kumamoto University, Kumamoto 860, Japan

References

1 LUGLI, P., and FERRY, D. K.: 'Degeneracy in the ensemble Monte-Carlo method for high-field transport in semiconductors', *IEEE Trans.*, 1985, **ED-32**, (11), pp. 2431–2437

2 FISCHETTI, M. V., and LAUX, S. E.: 'Monte-Carlo analysis of electron transport in small semiconductor devices including band-structure and space-charge effects', *Phys. Rev. B*, 1988, **38**, (14), pp. 9721–9745

PERFORMANCE CHARACTERISTICS OF GaInAs/GaAs LARGE OPTICAL CAVITY QUANTUM WELL LASERS

Indexing terms: Semiconductor lasers, Fibre optics, Optical fibres

The fabrication and performance characteristics of ridge-waveguide GaInAs/GaAs quantum-well lasers with large optical cavity (LOC) designs are reported. As expected, lasers with very large optical cavity have narrow far-field width (22°) perpendicular to the junction. However, due to small confinement factor, they also have higher threshold current (36mA). The LOC design has been optimised to produce lasers with low threshold current (12mA), high efficiency (0·45mW/mA/facet) and narrow far field divergence (32° × 12°). These lasers operate in the fundamental transverse mode to output powers of 130mW/facet.

Semiconductor lasers emitting near 0·98μm fabricated using $Ga_{0.8}In_{0.2}As/GaAs$ multi-quantum-well (MQW) structures are of considerable interest for application as pump lasers for erbium-doped glass fibre amplifiers.[1–5] Thus, in addition to high power output, high fibre coupling efficiency is an important parameter for the design of these lasers. High fibre coupling efficiency requires narrow far field. We have used a large optical cavity design to reduce the far field (by a factor of 2) normal to the junction plane of these lasers. This Letter reports the fabrication and performance characteristics of a large optical cavity ridge-waveguide laser emitting near 0·98μm.

The schematic cross-section of the $Ga_{0.8}In_{0.2}As/GaAs$ MQW ridge-waveguide laser is shown in Fig. 1. The active regions in these laser structures have one or many quantum wells with cladding layers of different composition around them. Three active region structures are shown in Fig. 1. They are grown by molecular beam epitaxy (MBE) growth technique on an n^+-GaAs substrate.

The MBE grown layers for Fig. 1*a* are (i) n^+-GaAs buffer layer, 0·5μm thick, (ii) N-$Al_{0.4}Ga_{0.6}As$ cladding layer, 1·5μm thick, (iii) N-$Al_{0.15}Ga_{0.85}As$ layer 400Å thick, (iv) MQW active region with three 80Å thick $Ga_{0.8}In_{0.2}As$ wells and four 60 Å thick GaAs barrier wells, (v) P-$Al_{0.15}Ga_{0.85}As$ layer, 400 Å thick, (vi) P-$Al_{0.3}Ga_{0.7}As$ cladding layer 2·0 μm thick, and (vii) P-GaAs contact layer, 0·1 μm thick. The $Al_{0.15}Ga_{0.85}As$ layers on either side of the MQW GaInAs active region are needed to form the large optical cavity. The different structures of active regions in Figs. 1*b* and *c* are self-explanatory.

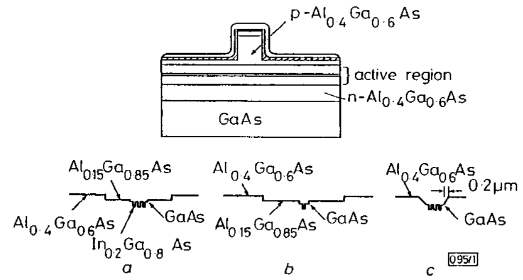

Fig. 1 *Schema of ridge-waveguide laser, showing the three active-layer designs*

After growth, 5 μm wide mesas are etched on the wafer using a photoresist etching mask and wet chemical etching. The mesas are oriented along the $\langle 1\bar{1}0 \rangle$ direction. The wafer is then processed using standard dielectric deposition and metallisation techniques to produce 500 μm long laser chips.

The intensity profile of the fundamental mode can be calculated[6] by solving the wave equation for the three structures shown in Fig. 1. The calculated full width at half maximum values for the three structures shown in Fig. 1 are 0·94 μm, 1·7 μm and 0·57 μm, respectively. The calculated mode profiles are shown in Fig. 2.

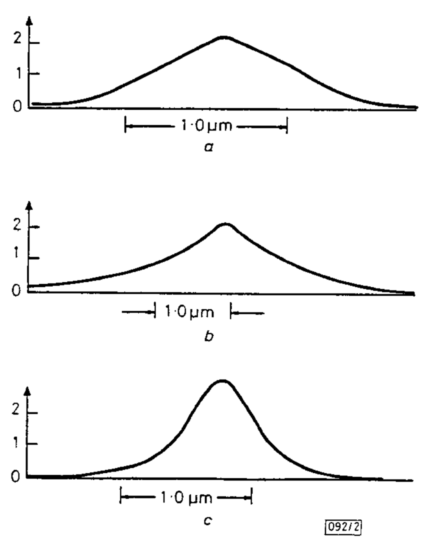

Fig. 2 *Calculated field intensity distribution normal to junction plane for three designs of Fig. 1*

The far field of a laser normal to the junction plane can be obtained from the intensity distribution of the propagating mode. For a Gaussian intensity profile of the form $e^{(-x^2/x_0^2)}$ for the propagating mode, the full width at half maximum (FWHM) of the far field is approximately given by[6]

$$\theta = 2 \sin^{-1}(0{\cdot}22\lambda/x_0) \tag{1}$$

The x_0 values are obtained by equating the FWHM obtained from Fig. 2 to that of a Gaussian distribution. The calculated θ_0 values, using eqn. 1 and calculated x_0 values, are 44°, 24° and 77° for Figs. 1*a*, *b* and *c*, respectively. The measured values for our devices are somewhat smaller, are discussed later. Note that the field intensity for the structure of Fig. 1*b* is significantly more spread out and can reach the contact metallisation, causing some absorption and therefore higher threshold and lower differential quantum efficiency unless the cladding layer is very thick.

The light/current characterisation of ridge-waveguide lasers fabricated using the three active layer designs of Fig. 1 is shown in Fig. 3. The designs *a*, *b* and *c* have threshold currents of 12, 36 and 16 mA, respectively. The carrier spreading was estimated to be $\sim 10 \mu m$ from the measurement of spontaneous emission. Hence a threshold current of 12 mA corresponds to a threshold current density of 240 A/cm^2. The external differential quantum efficiencies of designs *a* and *c* are comparable and are higher than that for *b*. The threshold currents for the designs *a* and *c* are similar. However, that for *b* is significantly larger. This may be due to small mode confinement for *b* compared with that for *a* and *c*. The mode confinement factor for *b* can be increased (by about a factor of 3) using three GaInAs quantum wells for the active region. This would increase the transparency current density by a factor of 3. But since the relationship of gain to current density is sublinear, the net effect may result in lower threshold than that shown in Fig. 3*b*. The absence of a kink in the plot of dL/dI against I indicates no change in transverse mode pattern.

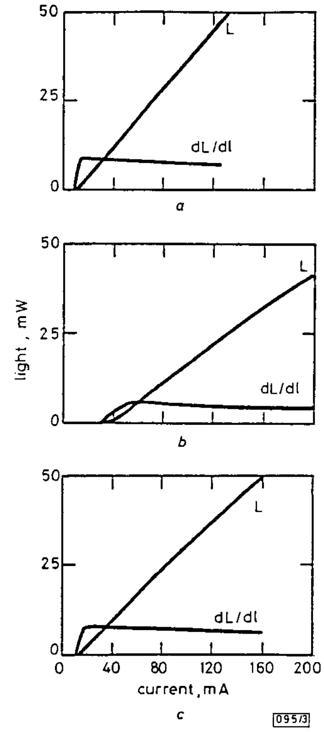

Fig. 3 *Measured light against current characterisation for three designs (Fig. 1)*

The measured intensity distribution of the far field along and normal to the junction plane is shown in Fig. 4 for the three designs. The far field along the junction plane for the three designs is similar (FWHM $\simeq$ 12°) because it is primarily determined by the weak index guiding provided by the ridge. However, normal to the junction plane the far-field widths vary significantly. The design 1*c* has the largest far-field width (FWHM $\simeq$ 68°) and design 1*a* has a FWHM far field width of 32° normal to the junction plane. The narrow far-field width is important for high fibre coupling efficiency. The light/current characteristics of design *a* at high currents are shown in Fig. 5.

In summary, we have optimised the design for a GaInAs/GaAs multi-quantum-well laser emitting near $0{\cdot}98\,\mu m$. Lasers with large optical cavity have narrow far-field width perpendicular to the junction plane. The optimised design has narrow far-field width ($32° \times 12°$), low threshold current (12 mA) and high efficiency (0·45 mW/mA/facet). The lasers emit in a fundamental transverse mode to output powers of

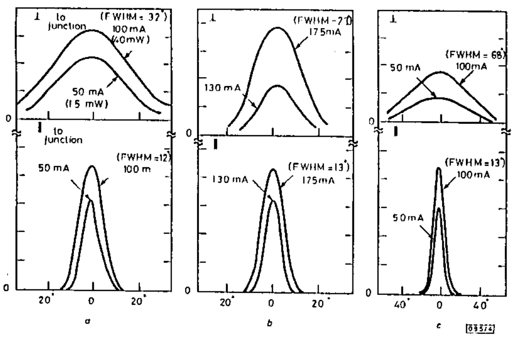

Fig. 4 *Measured far-field intensity profile along and normal to junction plane for three laser designs of Fig. 1*

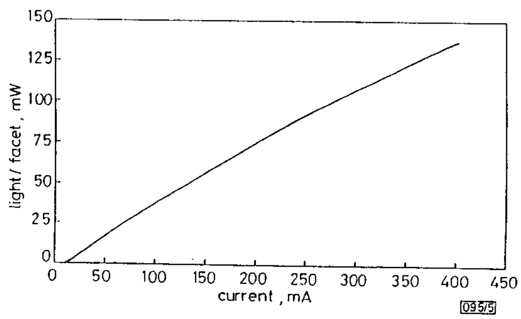

Fig. 5 *Light against current characteristics at high injection currents for a ridge waveguide laser fabricated using design a*

130 mW/facet. With a high reflectivity coating (>95%) at the back facet and a low reflectivity coating ($\sim 5\%$) on the front facet, the output power can be increased by almost a factor of two.

N. K. DUTTA
J. LOPATA
P. R. BERGER
D. L. SIVCO
A. Y. CHO

AT&T Bell Laboratories
Murray Hill, New Jersey 07974, USA

1st February 1991

References

1 YAMADA, M., SHIMIZU, M., TAKESHITA, T., OKAYASU, M., HORIGUCHI, M., UEHARA, S., and SUGITA, E.: 'Er doped fiber amplifier pumped by $0{\cdot}98\,\mu m$ laser diodes', *IEEE Photon. Tech. Lett.*, 1989, **1**, p. 422

2 WATERS, R. G., YORK, P. K., BEERNINK, K. J., and COLEMAN, J. J.: 'Viable strained layer laser at $\lambda = 1100$ nm', *J. Appl. Phys.*, 1990, **67**, p. 1132

3 LARSSON, A., FOROUHAR, S., CODY, J., and LANG, R. J.: 'High power operation of highly reliable narrow stripe pseudomorphic single quantum well laser at 980 nm', *IEEE Photon. Tech. Lett.*, 1990, **2**, pp. 307–309

4 WU, M. C., OLSSON, N. A., SIVCO, D. L., and CHO, A. Y.: 'A 970 nm strained layer InGaAs/GaAlAs quantum well laser for pumping Er amplifier', *Appl. Phys. Lett.*, 1990, **56**, pp. 221–223

5 DUTTA, N. K., WYNN, J. D., SIVCO, D. L., CHO, A. Y., and ZYDZIK, G. J.: 'Performance characteristics of InGaAs/GaAs quantum well lasers', *J. Appl. Phys.*, 1990, **68**, pp. 3822–3825

6 KRESSEL, H., and BUTLER, J. K.: 'Semiconductor lasers and heterojunction LEDs' (Academic Press, 1977)

EFFICIENT, NARROWBAND $LP_{01} \leftrightarrow LP_{02}$ MODE CONVERTORS FABRICATED IN PHOTOSENSITIVE FIBRE: SPECTRAL RESPONSE

Indexing terms: Convertors, Optical fibres

$LP_{01} \leftrightarrow LP_{02}$ mode convertors have been fabricated by photoinducing index gratings within the fibre core by means of internally or externally applied light fields. The mode convertors have conversion efficiencies of over 75% and simple spectral response curves with one or two peaks. The mode conversion linewidths range from 0·2 to 10 nm.

Introduction: A promising approach for fabricating fibre mode convertors is to create a periodic index grating in the core of an optical fibre using the fibre's photosensitive properties.[1] Mode convertor gratings fabricated using fibre photosensitivity have been demonstrated in a special two-mode elliptical core optical fibre.[2] In this case, high power 514·5 nm CW Ar-ion laser light is launched into the two modes of the fibre to produce a two-mode interference pattern that photoinduces an index grating of the correct period and cross-sectional shape. Since the writing light is guided within the fibre core, the procedure is referred to as the internal writing technique.

A drawback of the internal writing technique is that mode convertors cannot be designed to operate at preselected wavelengths that are relevant to optical fibre communication systems. This drawback has been overcome by using an external writing technique.[3] In this method, each element of the index grating is written point-by-point by photoinducing with ultraviolet light (249 nm) a small index perturbation in the fibre core. The technique is called external writing because the writing light irradiates the optical fibre from the side. Reference 3 reports the fabrication of an $LP_{01} \leftrightarrow LP_{11}$ mode convertor operating in the 600 to 900 nm wavelength region. Efficient intermodal coupling requires not only a grating of the correct period but also that the individual index perturbations be blazed.[3] That is the interface plane between perturbed and unperturbed index regions is tilted (blazed) at about 2 degrees to the optical fibre axis. The external writing technique has the advantage that mode convertors can be fabricated in standard optical fibre and operated at wavelengths appropriate to optical communication systems.

The externally written $LP_{01} \leftrightarrow LP_{11}$ mode convertors have, however, a complicated multiwavelength spectral response. The many peaks are a result of the LP_{11} approximate mode corresponding to four true modes in a fibre, i.e. the fibre is not really bimodal. In the fabrication of practical two-mode optical fibre devices, a mode convertor which operates in a narrow bandwidth about a single wavelength is preferable. Single peak spectral responses require two-mode fibres in which the higher order mode has only one mode constituent. This may be accomplished by using a special two-mode fibre as described in Reference 2 or by writing gratings that couple the LP_{01} to the LP_{02} mode whose corresponding two true modes are degenerate. The purpose of the paper is to report the fabrication of $LP_{01} \leftrightarrow LP_{02}$ mode convertors using both the internal and external writing techniques.

Internal writing: Fig. 1 shows the experimental configuration for fabricating the mode convertor grating. Light (488 nm) from an Ar-ion laser operating in a single longitudinal mode is launched into a fibre (normalised frequency $V = 6{\cdot}35$) and passed through a mode filter to leave only the LP_{01} mode in

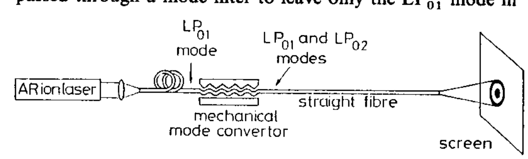

Fig. 1 *Schematic diagram of experimental arrangement used to write mode convertor gratings using the internal writing technique*